



# CHORUS

This is the accepted manuscript made available via CHORUS. The article has been published as:

## High-energy electron-helium scattering in a Nd:YAG laser field

B. A. deHarak, L. Ladino, K. B. MacAdam, and N. L. S. Martin

Phys. Rev. A **83**, 022706 — Published 10 February 2011

DOI: [10.1103/PhysRevA.83.022706](https://doi.org/10.1103/PhysRevA.83.022706)

# High-energy electron-helium scattering in a Nd:YAG laser field

B. A. deHarak,<sup>1</sup> L. Ladino,<sup>2</sup> K. B. MacAdam,<sup>2</sup> and N. L. S. Martin<sup>2</sup>

<sup>1</sup>*Physics Department, Illinois Wesleyan University,  
P.O. Box 2900, Bloomington, Illinois 61702-2900, USA*

<sup>2</sup>*Department of Physics and Astronomy,  
University of Kentucky, Lexington, Kentucky 40506-0055, USA*

## Abstract

We report measurements of the scattering of electrons by helium atoms in the presence of 1.17 eV photons from a Nd:YAG laser. The incident energy of the electrons was in the range 50 – 350 eV and the polarization of the laser was arranged to be parallel to electrons scattered through  $135^\circ$ . Energy-shifted peaks corresponding both to one- and two-photon emission were observed. Calculations using the Kroll-Watson approximation are perfectly consistent with the data.

PACS numbers: 34.80.Dp

## I. INTRODUCTION

The electron-atom collision process for an initial atom in the ground state  $A$ , an incident electron of energy  $E_i$ , a scattered electron of energy  $E_f$ , and a neutral final atomic state  $A'$ , may be written

$$A + e(E_i) \rightarrow A' + e(E_f). \quad (1)$$

The collisions may be divided into two main types: elastic and inelastic. In the former the atom is left in its ground state, and the electron loses almost no kinetic energy since the target is thousands of times more massive than the electron:  $E_f \approx E_i$ . In the latter the atom is left in an excited state  $A^*$ , lying  $\Delta E$  above the ground state, with a corresponding kinetic energy loss for the electron:  $E_f = E_i - \Delta E$ . The threshold energy is therefore  $E_i = \Delta E$ .

If an external radiation field of frequency  $\omega$  is present during the collision, there is the possibility of the absorption or emission of one or more photons, and the process may then be written

$$A + e(E_i) + \mathcal{N}\hbar\omega \rightarrow A' + e(E_f) + \mathcal{N}'\hbar\omega, \quad (2)$$

where  $\mathcal{N}' = \mathcal{N} \pm n$ , corresponding to the emission (+) or absorption (−) of  $n$  photons by the  $A + e$  system.

As in reaction (1), the final atomic state may be the initial ground state or an excited state. Thus there are two processes equivalent to those above when no external radiation field is present. The so called “free-free” transition case ( $A' = A$ ) is where the elastic scattering process provides a mechanism for both energy and momentum conservation as the electron absorbs or emits  $n$  photons in the field of the atom, resulting in a final electron kinetic energy  $E_f = E_i \pm n\hbar\omega$ . The inelastic scattering analog ( $A' = A^*$ ) is known as “Simultaneous Electron-Photon Excitation”, or SEPE [1], where the  $A+e$  system absorbs or emits  $n$  photons during electron-impact excitation and the electron’s final energy is  $E_f = E_i - \Delta E \pm n\hbar\omega$ . For absorption, the threshold energy is thus lower than the radiation-free case:  $E_i = \Delta E - n\hbar\omega$ , *i.e.*, the classic signature of SEPE is a lower electron-impact onset for excitation.

The first experiments involving electron scattering in a laser field were carried out on free-free transitions using a CO<sub>2</sub> laser (photon energy 0.117 eV) during e–Ar elastic scattering. Andrick and Langhans [2] observed sidebands in the energy-loss signal corresponding to the absorption and emission of a single photon, and Weingartshofer *et al.* [3] observed the absorption and emission of up to three photons. Wallbank and Holmes [4] carried out similar

experiments using a pulsed CO<sub>2</sub> laser and a helium target. They reported the absorption and emission of up to five 0.117 eV photons. The first SEPE experiments were carried out by Mason and Newell [5] who observed the lowering of the excitation threshold of He 2<sup>3</sup>S by detecting these metastables as a function of incident electron energy when CO<sub>2</sub> laser photons were present. Luan *et al.* [6] investigated SEPE in He using a Nd:YAG laser which produces photons of energy 1.17 eV, ten times the CO<sub>2</sub> laser energy. A comprehensive review of later free-free and SEPE work has been given by Mason [1] in 1993, and a more recent review of theory is given by Ehlötzky, Jaroń, and Kamiński [7].

A theoretical model that has been widely compared with free-free experimental data is the Kroll-Watson approximation (KWA) [8], in which quantum-mechanical scattering theory is applied to an electron in an (unquantized) electromagnetic field. It is particularly appealing since it has a simple analytical form which relates the free-free cross section, for absorption or emission of  $n$  photons, to the field-free elastic-scattering cross section. The main assumption of the Kroll-Watson approximation is that the laser-atom interaction can be neglected; *i.e.*, the sole purpose of the presence of the atom is to allow the conservation of both energy and momentum during the absorption or emission of the  $n$  photons by the electron. In addition, there are two regimes when the approximation is applicable. The first is the *soft-photon* limit when  $n\hbar\omega/E_i \ll 1$ . The second is when the Born approximation may be used for the field-free elastic-scattering cross section, in which case there are no restrictions on  $n\hbar\omega/E_i$ .

In light of these assumptions, free-free experiments may be separated into two categories: those where the Kroll-Watson approximation is expected to be valid, and those where it is not. At the time that Mason's review was written, the Kroll-Watson approximation had been found to be in agreement with all experimental data of the former type [1]. Since then its limits have been probed by experiments of the latter type; see [9] for details.

The soft-photon limit was examined by Wallbank and Holmes [10] in free-free experiments using 0.117 eV photons and an electron beam of energy as low as 0.2 eV. It was found that the experimental effect was about a factor of five lower than the Kroll-Watson approximation prediction. Some of this disagreement may have been due to uncertainties in the exact spatial profile of the laser beam, but there were also features in the incident-energy dependence of the free-free signal that could not be reproduced by Kroll-Watson approximation calculations, even when these were carried out for a variety of laser modes and intensities. At the lowest incident energy, the Kroll-Watson approximation predicts

that the free-free signal for absorption and emission should be very different, with a ratio of one-photon absorption to one-photon emission of about 3.5. The measured ratio was about 2, in agreement with a more sophisticated calculation, which however, failed to reproduce the absolute magnitudes of the cross sections [10].

The neglect of the laser-atom interaction can be investigated by experiments carried out with high laser power, but under conditions where the Kroll-Watson approximation predicts very small, or indeed vanishing, free-free cross sections. Wallbank and Holmes carried out a free-free experiment for electrons scattered through  $9^\circ$ , for which the Kroll-Watson approximation predicts a small cross-section [4, 11]. It was found that the Kroll-Watson approximation underestimated the free-free cross sections by orders of magnitude. In other experiments [12] they chose a geometry where the laser polarization was perpendicular to the momentum transfer of the collision. The free-free signal was as high as 12% of the elastic peak, whereas the Kroll-Watson approximation predicted zero free-free cross section.

There is still much interest in the applicability of the Kroll-Watson approximation. A very recent study [13] compared a Kroll-Watson approximation calculation with a sophisticated  $R$ -matrix Floquet calculation of the free-free cross-section for 22 eV electrons scattered from helium through angles from  $20^\circ$  to  $70^\circ$ . The two calculations were in excellent agreement with each other and with the experimental data. Most recently the Kroll-Watson approximation has been applied to free-free experiments using a molecular target [14].

Almost all experimental investigations of the Kroll-Watson approximation to date have been carried out for incident electron energies of less than 40 eV and with 0.117 eV photons. In this paper we present the results of our free-free experiments on electron helium scattering for a range of incident energies between 50 and 350 eV, in the presence of 1.17 eV photons from a pulsed Nd:Yag laser. Thus our experiments lie in a region expected to be well described by Kroll-Watson, but one that has never been tested.

Section II gives the Kroll-Watson approximation, and Section III describes the apparatus and the geometry of our free-free measurements. Section IV presents the results, and Section V our conclusions.

## II. THEORY

The Kroll-Watson approximation relates the free-free cross section  $d\sigma_{FF}^{(n)}/d\Omega$ , for absorption ( $n < 0$ ) or emission ( $n > 0$ ) of  $n$  photons, to the field-free elastic-scattering cross section  $d\sigma_{el}/d\Omega$ , by [8]

$$\frac{d\sigma_{FF}^{(n)}}{d\Omega} = \frac{k_f}{k_i} J_n^2(x) \frac{d\sigma_{el}}{d\Omega}. \quad (3)$$

Here  $\mathbf{k}_i$  and  $\mathbf{k}_f$  are the initial and final electron momenta, and  $J_n$  is a Bessel function of the first kind of order  $n$ , whose argument is given by

$$x = -0.022\lambda^2 I^{1/2} E_i^{1/2} \frac{\hat{\boldsymbol{\epsilon}} \cdot \mathbf{Q}}{k_i}, \quad (4)$$

where  $\lambda$  is the wavelength of the radiation in  $\mu\text{m}$ ,  $I$  is its intensity in  $\text{GW}/\text{cm}^2$ ,  $\hat{\boldsymbol{\epsilon}}$  is the polarization direction,  $E_i$  is the incident electron energy in eV, and  $\mathbf{Q} = \mathbf{k}_f - \mathbf{k}_i$  is the momentum transfer.

In the limit of small  $x$ , the Bessel function may be approximated by the first term of a power series expansion and Eq. (3) becomes

$$\frac{d\sigma_{FF}^{(n)}}{d\Omega} \approx \frac{k_f}{k_i} \left( \frac{1}{|n|!} \right)^2 \left( \frac{x}{2} \right)^{2|n|} \frac{d\sigma_{el}}{d\Omega}. \quad (5)$$

For the experiments reported below, this form is not applicable since  $x$  is not small. However it is useful since it shows that the Kroll-Watson approximation predicts very small, or indeed vanishing, free-free cross sections under certain circumstances. Eq. (5) shows that this occurs for small  $x$ , and, since  $x \propto \hat{\boldsymbol{\epsilon}} \cdot \mathbf{Q}$ , there are two simple possible experimental ways of achieving this. Thus for the experiments of Wallbank and Holmes referred to above, the  $9^\circ$  scattering experiment [4, 11] corresponds to small  $Q$  (and  $\hat{\boldsymbol{\epsilon}}$  almost perpendicular to  $\mathbf{Q}$ ), and the other experiment [12] has  $\hat{\boldsymbol{\epsilon}} \cdot \mathbf{Q} = 0$ .

Figure 1 shows one-photon and two-photon free-free cross sections calculated using Eq. (3), with a scattering angle  $135^\circ$ , incident energies up to 350 eV, and sample laser intensities of 3, 6, and 9  $\text{GW}/\text{cm}^2$  and polarization parallel to the scattered-electron direction. At the lowest laser intensity the one-photon cross section increases monotonically with incident energy, but, at the highest intensity, the cross section has a maximum at about 200 eV. On the other hand the two-photon free-free cross sections all increase with increasing energy. As a result, all the one-photon cross sections are close to each other in magnitude in the region above 300 eV, whereas the corresponding two-photon cross sections are very

different in this region. Figure 2 shows the two-photon to one-photon free-free cross-section ratio at 300 eV incident energy as a function of laser intensity. The increase in the ratio with intensity indicates that a measurement of the ratio at 300 eV can be used to deduce the laser intensity within the validity of the Kroll-Watson approximation.

### III. EXPERIMENTAL

The free-free experiments were carried out using an electron spectrometer interfaced with a Continuum Powerlite 9030 Nd:YAG laser. This has a photon energy 1.17 eV ( $\lambda=1.06 \mu\text{m}$ ), a repetition rate of 30 Hz, a pulse duration of 6 ns, and, in the present experiments, a measured energy of 0.13 J per pulse. The laser beam enters the vacuum system through an infrared window, followed by a lens positioned so as to produce a nominal beam diameter of 0.75 mm measured in the interaction region using burn paper. The laser beam is terminated in a beam dump outside the vacuum system. A schematic of the experimental set up is shown in fig. 3. The electron spectrometer is an extensively modified version of an apparatus previously used for  $(e,2e)$  studies [15, 16]. It consists of an unmonochromated electron gun and a scattered electron detector, mounted on independent concentric turntables, a single-bore gas nozzle to create the helium beam, and a Faraday cup to collect the electron beam.

The electron gun is from a high-current-output design by Erdman and Zipf [17]. The main difference is the addition of an exit tube, 0.5 cm long and 0.75 mm internal diameter, whose tip is located as close to the interaction region as possible (*i.e.*, without the gun assembly being struck by the laser beam). In this way a well collimated electron beam of known diameter and trajectory is produced. The unmonochromated electron beam has an energy width of approximately 0.5 eV, and therefore the field-free intensity is relatively small in the wings one photon energy (1.17 eV) away from the elastic peak, and does not unduly degrade the statistics of the free-free signal. (This is an advantage over free-free experiments using the 0.117 eV photons from a CO<sub>2</sub> laser, where a monochromated electron beam is essential.)

The scattered-electron detector is actually the ejected-electron spectrometer from the  $(e,2e)$  apparatus; the electron optics, consisting of lens elements and a hemispherical-sector energy analyzer, are shown in ref. [15]. The energy analyzer is now terminated in a resistive anode which is part of a position sensitive detector (PSD) [18]. For the present experiments

the energy window of the system was set to be 0.5 eV, corresponding to the energy width of the electron beam.

The gas nozzle has an internal diameter of 1 mm and is positioned 3 mm below the interaction region formed by the intersection of the electron and laser beams, and we estimate an effective helium beam diameter of approximately 3 mm. The insert in fig. 3 shows a schematic close up of the interaction region. The sum of the three volumes  $V_A + V_B + V_C$  all contribute to the elastic-scattering peak that is accepted by the scattered-electron detector, but only the volume  $V_B$  contributes to the observed free-free signal. Thus, when modelling our results, we need to multiply the theoretical values by an overlap factor  $\mathcal{R}$ , which, in the simple case illustrated in the figure, is given by the ratio of the volumes,

$$\mathcal{R} = \frac{V_B}{V_A + V_B + V_C}. \quad (6)$$

The actual value of  $\mathcal{R}$  depends on the assumed profile of the laser beam. When presenting our results we will consider the two cases of a uniform, and a Gaussian, radial intensity profile. From fig. 3 we expect the real value of  $\mathcal{R} \lesssim 1/3$ .

The output of the PSD is fed to the data acquisition system (DAQ); details of the DAQ will be given elsewhere. It is a simple, versatile system based on the Parallax Inc. Propeller<sup>TM</sup> microcontroller [19] with an 80 MHz clock, and hence a time resolution of 12.5 ns. In our experiments, carried out with a continuous electron beam, it is necessary to record the arrival times of scattered electrons relative to the laser pulse, in order to distinguish between *laser-on* and *laser-off* events. The laser is triggered by signals from a Stanford Research Systems DG535 Digital Delay/Pulse Generator [20], which also provides a separate, synchronized, pulse used for timing reference by the DAQ. Each PSD event is then allocated a *timestamp* which is the 12.5 ns bin in which it occurs. The PSD is gated so that data is collected for 400  $\mu$ s (*i.e.*, 32,000 time bins) with the free-free signal occurring in the central region.

Figure 4 is a schematic showing the quantities measured. The *laser-off* signal,  $Q$  in the figure, corresponds to the intensity of the low-energy wing of the main elastic peak, 1 photon energy away from the center, and the *laser-on* signal  $P$  also includes the free-free signal. Figure 5 shows a portion of a resultant timing spectrum when the detector pass energy is set one photon energy below the elastic-scattering peak of 100 eV incident electrons. The free-free signal occupies several 12.5 ns time bins; although the laser pulse is 6 ns, there

is a time spread of electron trajectories through the analyzer optics [21]. The net free-free signal is not directly given by the area of the peak above the background; a small correction needs to be made because the *laser-on* background is slightly different from the *laser-off* background. This is described in the Appendix.

Below we present our data as the ratio (free-free rate)/(elastic-scattered rate). Before and after each experiment the elastic-scattering rate (for the energy window  $R$  in fig. 4) was measured using the PSD output. The rates were very high, up to several hundred thousand counts per second, and it was necessary to apply a dead-time correction.

#### IV. RESULTS AND DISCUSSION

Free-free experiments, corresponding to one-photon emission, were carried out at incident electron energies from 50 eV to 350 eV, in 50 eV intervals. In addition a two-photon emission measurement was made for 300 eV. For all experiments the energy of a laser pulse was 0.13 J, corresponding to a peak power of approximately 20 MW. The experimental setup was as shown in fig. 3, with the scattered-electron detector aligned with the laser polarization, and a scattering angle of  $135^\circ$ .

Figure 6 shows our results. We plot the measured ratio free-free rate/elastic-scattering rate, where the free-free rate incorporates the corrections of Eqs. (A2) & (A3), and the elastic-scattering rate is the rate measured when the laser is off. This ratio corresponds to the quantity  $\mathcal{R}(d\sigma_{FF}^{(n)}/d\Omega)/(d\sigma_{el}/d\Omega)$  with  $n = 1$  and  $2$ . The total uncertainty of each data point consists of the statistical uncertainty combined in quadrature with an estimated systematic uncertainty of 10%. The latter includes an uncertainty in the dead-time correction of the elastic-scattered count rate, and any drift in the experiment over the approximately 24 hours required for each measurement.

We cannot directly compare our results with the Kroll-Watson approximation Eq. (3) since we do not know the precise laser-beam profile or the interaction-region overlap factor  $\mathcal{R}$ . We have therefore tested the *consistency* of our results and the Kroll-Watson approximation by assuming it is correct at 300 eV, deriving the required parameters, and then comparing the energy dependence of the calculated cross section with our experimental results. In the Kroll-Watson approximation  $d\sigma_{el}/d\Omega$  and  $k_f$  are meant to be evaluated at the final electron energy. However, our incident electron energies are much greater than the photon energy

and we therefore assume that these are the same as those evaluated at the incident energies.

The ratio of two-photon to one-photon free-free rates are then given by  $(J_2(x)/J_1(x))^2$ , which enables us to find  $x$  and hence the laser intensity  $I$ . The measured ratio is 0.26 which corresponds to a laser intensity 5.6 GW/cm<sup>2</sup> (see fig. 2). Assuming a constant spatial laser profile, this yields a laser-beam diameter of 0.70 mm, within 10% of the 0.75 mm estimate obtained from the burn-paper measurement. Using the deduced laser power in Eq. (3) gives  $(d\sigma_{FF}^{(1)}/d\Omega)/(d\sigma_{el}/d\Omega) = 0.337$  for an incident energy of 300 eV. Comparing this with our 1-photon free-free measurement yields an overlap factor  $\mathcal{R} = 0.27$ , which only differs by 20% from our estimate of  $\sim 1/3$ .

The curves in fig. 6 show the resultant values of  $\mathcal{R}(d\sigma_{FF}^{(n)}/d\Omega)/(d\sigma_{el}/d\Omega)$  for  $n = 1$  and 2, calculated using the Kroll-Watson approximation. They are in excellent agreement with the experimental results over the full incident-electron energy range of 50 to 350 eV. Note that, like the 6 GW/cm<sup>2</sup> curve in fig. 1, the 1-photon emission cross section reaches its maximum value at about 350 eV.

The scale on the right of fig. 6 gives the actual calculated cross-section ratio  $(d\sigma_{FF}^{(n)}/d\Omega)/(d\sigma_{el}/d\Omega)$ , with a maximum value of 1/3 for the 1-photon emission cross section. In fact the Kroll-Watson approximation predicts that the  $n = 0$  elastic peak will be depleted by over 90%, with roughly 2/3 going to  $n = \pm 1$ . Thus our correction to the data embodied in Eq. (A3) is somewhat underestimated since we do not include  $|n| > 1$ , but any inaccuracy is taken care of by the 10% systematic uncertainties.

The above calculations assume a constant spatial and temporal laser profile. We have also taken a model where the spatial or temporal intensity profile is assumed to be a Gaussian of the form

$$I = \frac{I_0}{\sqrt{2\pi}\chi} e^{-\frac{1}{2}\left(\frac{y}{\chi}\right)^2}, \quad (7)$$

where  $y = r$  or  $t$ . In both cases we were able to choose realistic parameters  $I_0, \chi$  which resulted in curves almost identical to those shown in fig. 6. The temporal profile was taken as a Gaussian of full width at half maximum (FWHM) of 6ns. The spatial profile had an FWHM diameter of 0.73 mm, and, when the integral was taken for  $r = 0 \rightarrow 2\chi$ , an overlap factor  $\mathcal{R} = 0.33$ .

## V. CONCLUSIONS

We have demonstrated that the Kroll-Watson approximation is perfectly consistent with all our experimental results from 50 to 350 eV incident electron energies. Furthermore, the fitted parameters used in the calculations (laser radius and overlap), are in very good agreement with our initial estimates. Our results are also consistent with more sophisticated models that take into account the temporal or spatial shape of a laser pulse.

### Acknowledgments

This work was supported by the United States National Science Foundation under Grant No. PHY-0855040. We thank W. L. Fuqua III and T. G. Porter for developing the data acquisition system.

### Appendix A

In what follows,  $X^{(n)}$  refers to a quantity that has been measured  $n$  photon energies away from the center of the elastic peak. Thus, for example,  $N_{\text{off}}^{(0)}$  refers to a measurement of the central portion of the total elastic peak ( $R$  in fig. 4) that is accepted by the electron detector, rather than the total energy-integrated elastic peak.

In fig. 5 the net counts above the background are

$$N = \sum_{\nu} (N_{\text{on}}^{(1)} - N_{\text{off}}^{(1)}) \pm \sqrt{\sum_{\nu} N_{\text{on}}^{(1)}}, \quad (\text{A1})$$

where  $N_{\text{on}}^{(n)}$  are the *laser-on* counts and  $N_{\text{off}}^{(n)}$  is the average background count per time bin ( $P$  and  $Q$ , respectively, in fig. 4). The sums in Eq. (A1) extend over the  $\nu$  time bins occupied by the peak – six in the case of fig. 5. The statistical uncertainty assumes that there is no uncertainty in the average background, since it is computed from thousands of time bins.

Equation (A1) does not directly give the free-free counts since it ignores the change in the intensity of the wings themselves due to free-free transitions. If the *laser-off* count in the wings is a fraction  $\alpha^{(n)}$  of the measured elastic-peak count  $N_{\text{off}}^{(0)}$ , then  $N_{\text{off}}^{(n)} = \alpha^{(n)} N_{\text{off}}^{(0)}$ , and the *laser-on* background count for  $n = 1$  needs to be reduced by  $\alpha^{(1)} \sum_{|n|>0} N_{\text{free-free}}^{(n)}$ , where  $\alpha^{(1)}$  is (Area Q)/(Area R) in fig. 4. . The net free-free signal for electrons that have

emitted one photon is thus given by

$$N_{\text{free-free}}^{(1)} = \sum_{\nu} (N_{\text{on}}^{(1)} - N_{\text{off}}^{(1)}) + \alpha^{(1)} \sum_{|n|>0} N_{\text{free-free}}^{(n)} \pm \sqrt{\sum_{\nu} N_{\text{on}}^{(1)}}, \quad (\text{A2})$$

which cannot be solved without measuring all orders  $n$  of free-free transitions. We can obtain an approximation by assuming that only the  $n = \pm 1$  correction is significant (and that the elastic peak is approximately symmetric), in which case

$$N_{\text{free-free}}^{(1)} = \frac{1}{1 - 2\alpha^{(1)}} \left( \sum_{\nu} (N_{\text{on}}^{(1)} - N_{\text{off}}^{(1)}) \pm \sqrt{\sum_{\nu} N_{\text{on}}^{(1)}} \right), \quad (\text{A3})$$

which differs from Eq. (A1) by the factor  $1/(1 - 2\alpha^{(1)})$ ; for our experimental values of  $\alpha^{(1)}$  at the various incident energies, we find a maximum correction factor of 1.05. Using similar reasoning we find that for 2-photon emission

$$N_{\text{free-free}}^{(2)} = \sum_{\nu} (N_{\text{on}}^{(2)} - N_{\text{off}}^{(2)}) - (\alpha^{(1)} 2\alpha^{(2)}) N_{\text{free-free}}^{(1)} \pm \sqrt{\sum_{\nu} N_{\text{on}}^{(2)}}, \quad (\text{A4})$$

which results in a correction of slightly under 4% to our datapoint for 300 eV incident energy. Note that the above corrections do not depend on the value of  $\mathcal{R}$ .

The above discussion ignores possible *increases* to the background due to, for example, the  $n = 2$  contribution of the high-energy wing one photon energy above the elastic peak. The situation is further complicated by the asymmetric nature of an elastic peak from an unmonochromated thermionic source. We believe that eqs. (A3) & (A4) represent the simplest first-order corrections that can be made.

- 
- [1] N. J. Mason, Rep. Prog. Phys. **56**, 1275 (1993).
  - [2] D. Andrick and L. Langhans, J. Phys. B **9**, L459 (1976).
  - [3] A. Weingartshofer, J. K. Holmes, G. Caudle, E. M. Clarke, and H. Krüger, Phys. Rev. Lett. **39**, 269 (1977).
  - [4] B. Wallbank and J. K. Holmes, Phys. Rev. A **48**, R2515 (1993).
  - [5] N. J. Mason and W. R. Newell, J. Phys. B **20**, L323 (1987).
  - [6] S. Luan, R. Hippler, and H. O. Lutz, J. Phys. B **24**, 3241 (1991).
  - [7] F. Ehlotzky, A. Jaroń, and J. Kamiński, Physics Reports **297**, 63 (1998).

- [8] N. M. Kroll and K. M. Watson, Phys. Rev. A **8**, 804 (1973).
- [9] S. Geltman, Phys. Rev. A **53**, 3473 (1996).
- [10] B. Wallbank and J. K. Holmes, J. Phys. B **29**, 5881 (1996).
- [11] B. Wallbank and J. K. Holmes, J. Phys. B **27**, 1221 (1994).
- [12] B. Wallbank and J. K. Holmes, J. Phys. B **27**, 5405 (1994).
- [13] D. Nehari, J. Holmes, K. M. Dunseath, and M. Terao-Dunseath, J. Phys. B **43**, 025203 (2010).
- [14] M. O. Musa, A. MacDonald, L. Tidswell, J. Holmes, and B. Wallbank, J. Phys. B **43**, 175201 (2010).
- [15] N. L. S. Martin and D. B. Thompson, J. Phys. B **24**, 683 (1991).
- [16] N. L. S. Martin, R. P. Bauman, and M. Wilson, Phys. Rev. A **59**, 2764 (1999).
- [17] P. W. Erdman and E. C. Zipf, Rev. Sci. Instr. **53**, 225 (1982).
- [18] B. A. deHarak, J. G. Childers, and N. L. S. Martin, J. Elec. Spec. Rel. Phen. **141**, 75 (2004).
- [19] <http://www.parallax.com>.
- [20] <http://www.thinksrs.com>.
- [21] R. E. Imhof, A. Adams, and G. C. King, J. Phys. E: Sci. Instr. **9**, 138 (1976).

FIG. 1: (colour online). Kroll-Watson approximation calculations for free-free transitions at incident-electron energies 50 to 350 eV. The scattering angle is  $135^\circ$  and the laser polarization is parallel to the scattered electron direction. The upper three curves are for 1-photon emission, and the lower three curves are for 2-photon emission. The dashed, solid, and chained lines correspond to laser intensities 3, 6, and 9 GW/cm<sup>2</sup>, respectively.

FIG. 2: (colour online). Calculated ratio of 2-photon to 1-photon emission free-free cross sections as a function of laser intensity for 300 eV incident electrons. The scattering angle and laser polarization are the same as in fig. 1.

FIG. 4: (colour online). Left panel: schematic of *laser-on* energy profile of scattered electrons. Right panel: schematic of *laser-off* energy profile. The areas  $P, Q, R$  correspond to the quantities measured during an experiment.

FIG. 5: (colour online). Timing spectrum of scattered-electron events with 1.17 eV energy loss from a 100 eV incident electron beam, showing the counts per 12.5ns time bin. The dashed line is to guide the eye.

FIG. 3: (colour online). Schematic of the apparatus used for the free-free measurements. The insert shows a simple model of the interaction region, indicating the overlap of the electron beam and the helium beam (volumes A,B,C), and the overlap of all three beams (volume B).

FIG. 6: (colour online). Free-free transitions at incident-electron energies 50 to 350 eV. The scattering angle is  $135^\circ$  and the laser polarization is parallel to the scattered electron direction. The solid circles are the experimental data for 1-photon emission, and the solid square is for 2-photon emission. The error bars include both statistical uncertainties and a systematic error of 10%. The solid lines are 1-photon and 2-photon Kroll-Watson approximation calculations fitted to our experiment at 300 eV. See text for details.

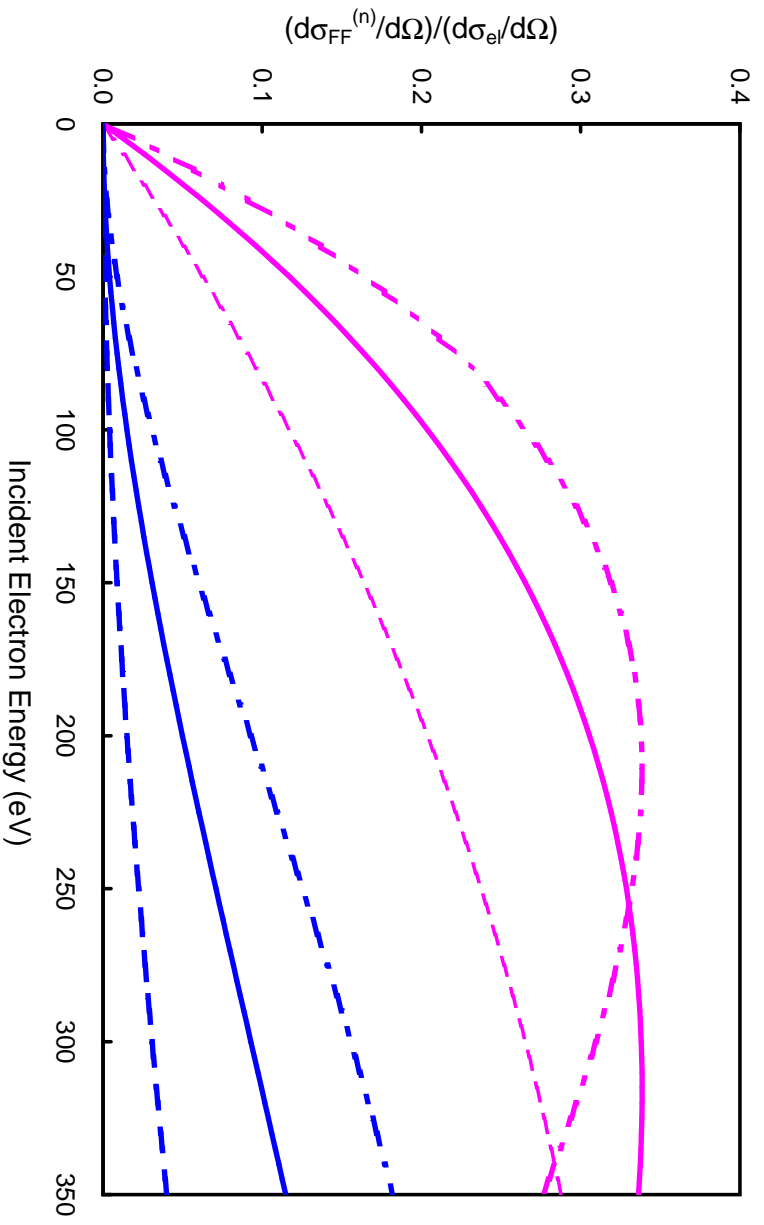


Figure 1 AZ110525 06Jan2011

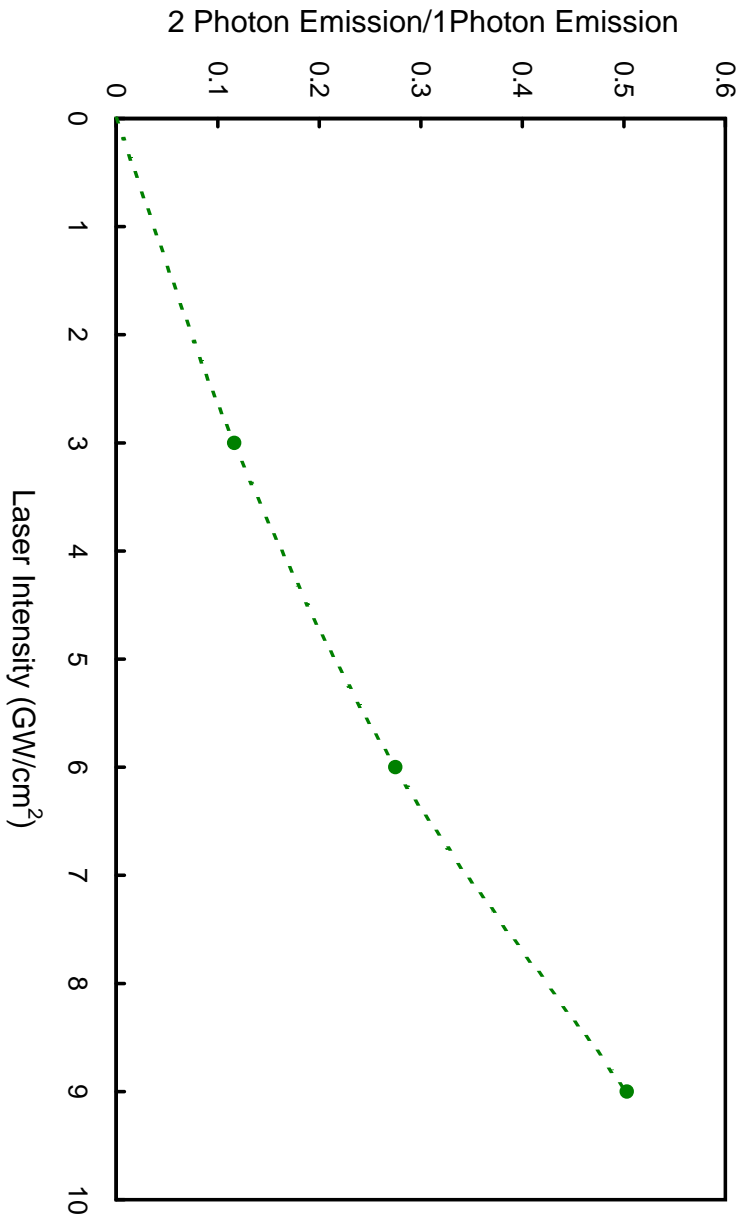


Figure 2 AZ10525 06Jan2011

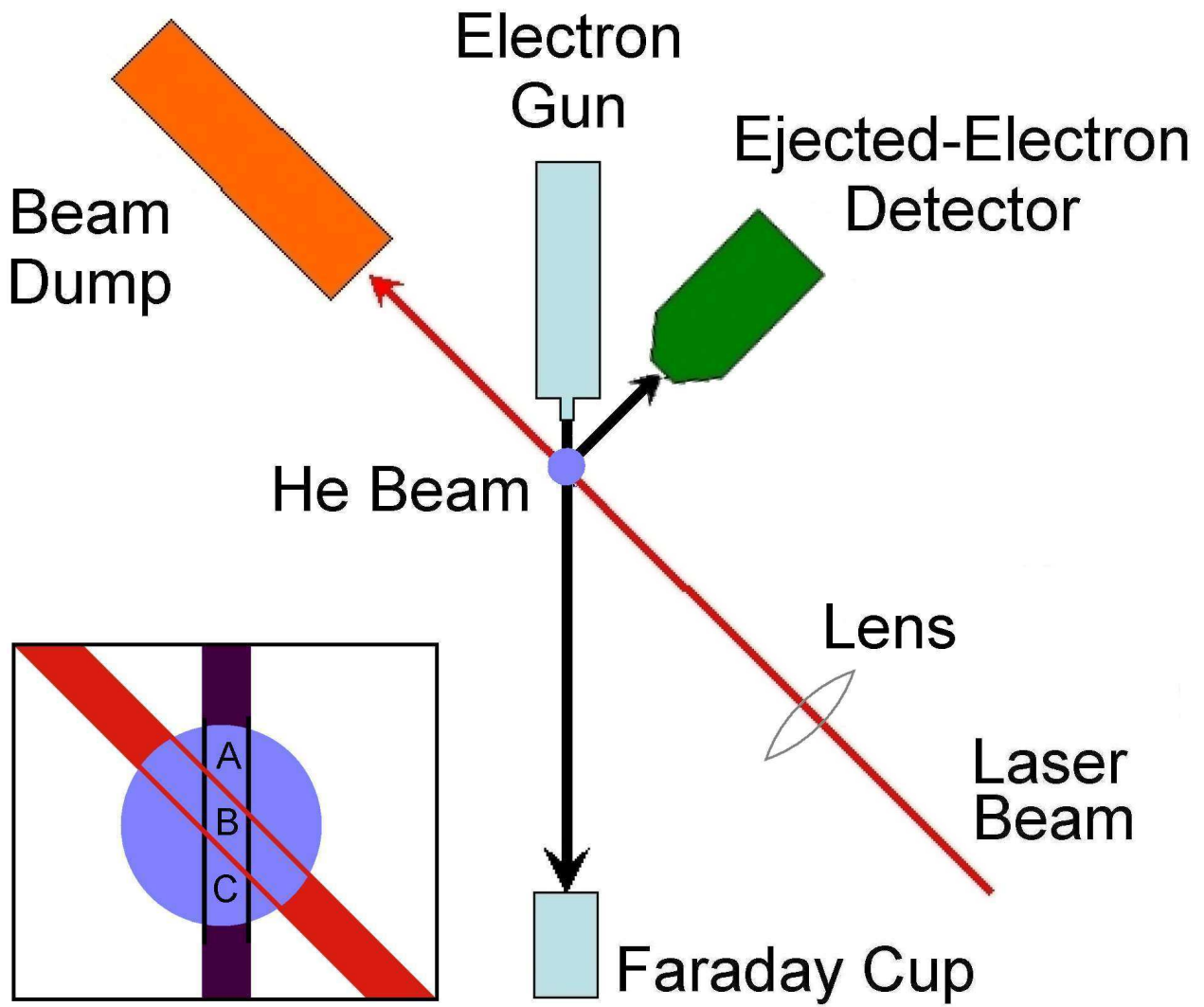


Figure 3

AZ10525

06Jan2011

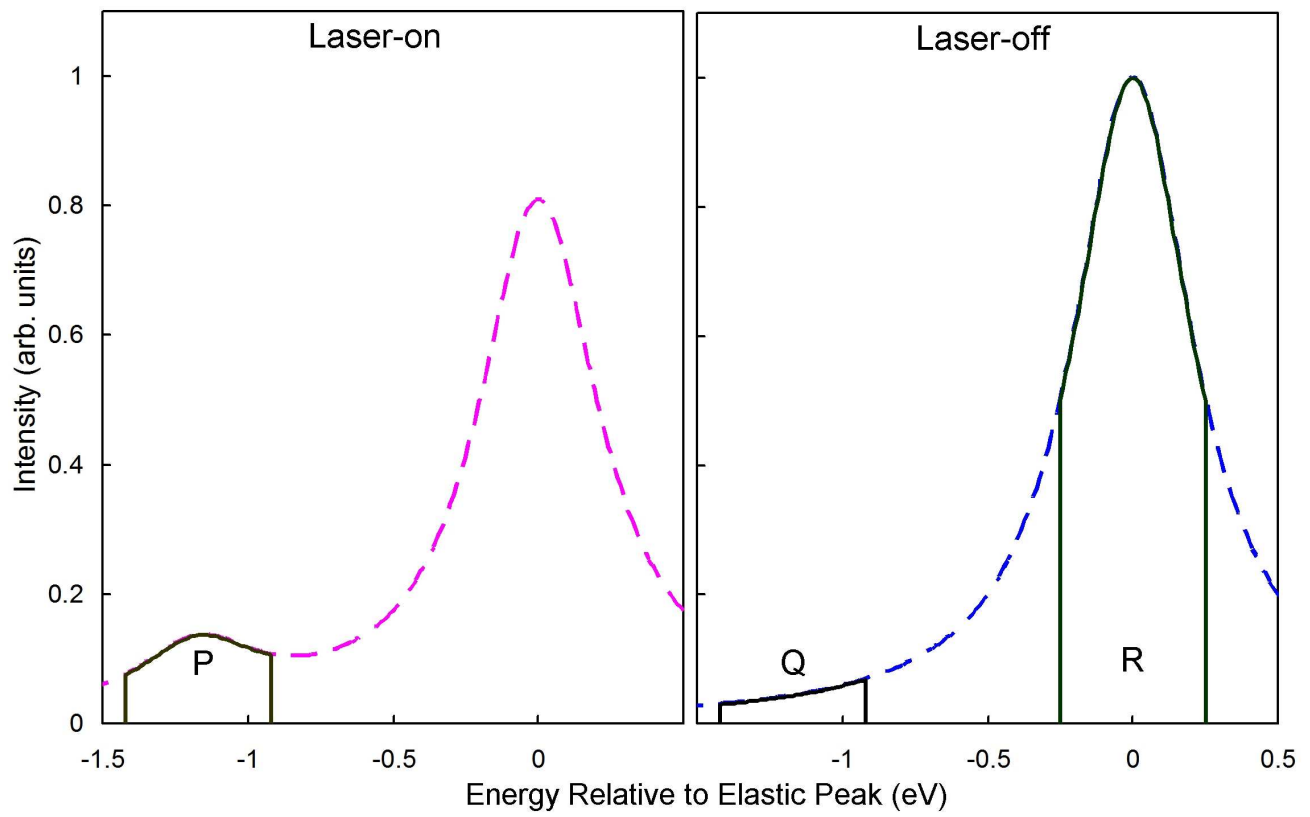


Figure 4 AZ10525 06Jan2011

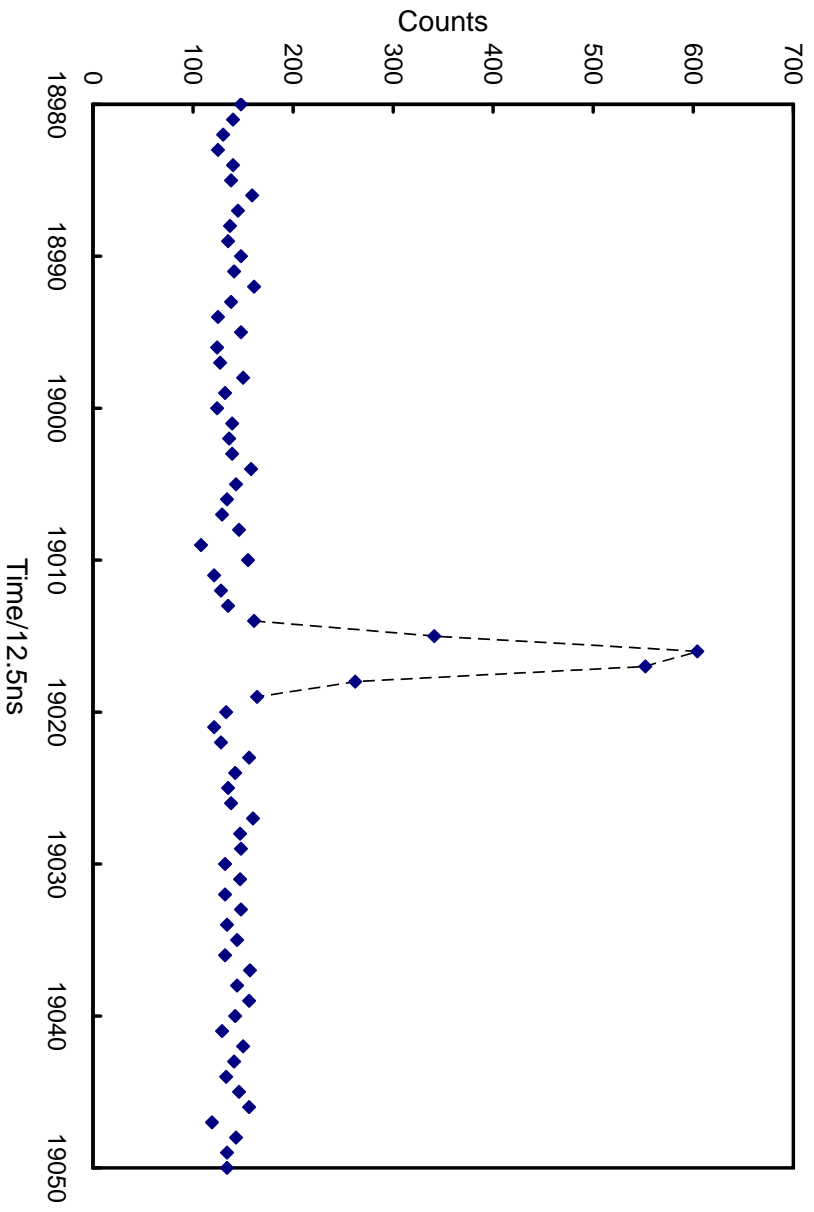


Figure 5 AZ10525 06Jan2011

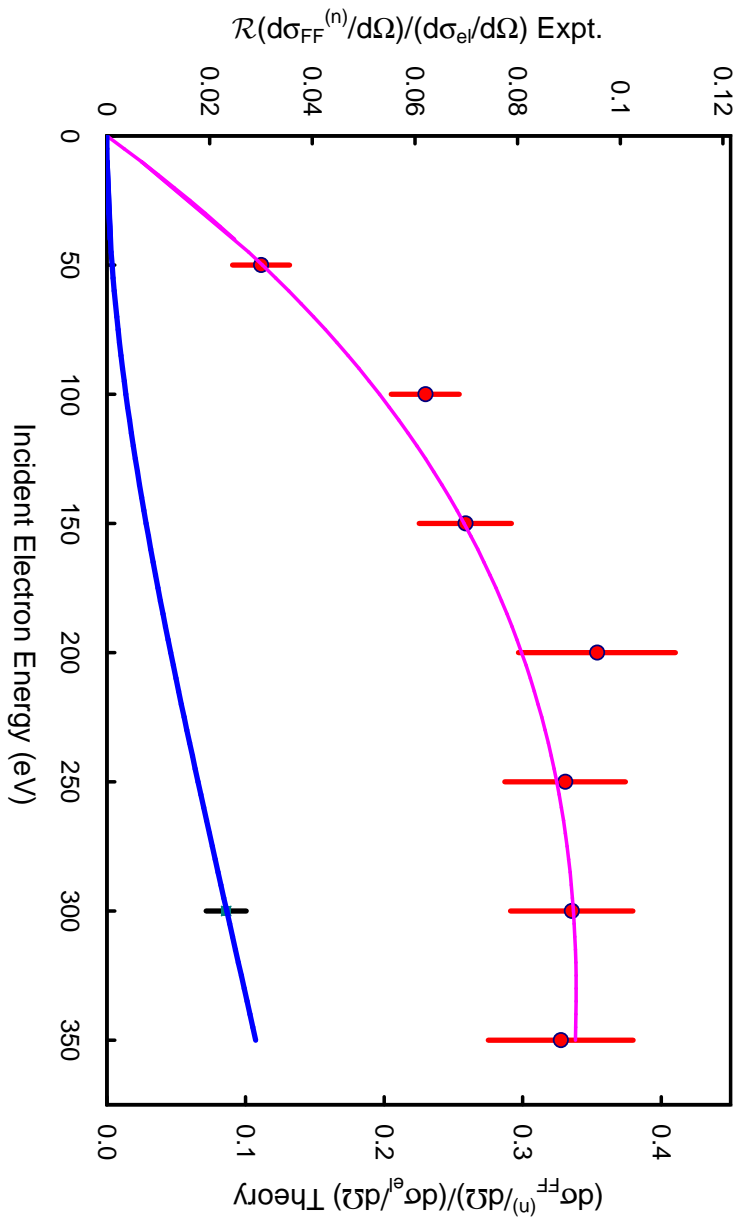


Figure 6 AZ10525 06Jan2011